Thermally Induced Aggregation of Human Transferrin Receptor Studied by Light-Scattering Techniques

Jens Schüler, Joachim Frank, Wolfram Saenger, and Yannis Georgalis
Institut für Kristallographie, Freie Universität Berlin, D-14195 Berlin, Germany

ABSTRACT The thermal stability of transferrin receptor isolated from human placenta in detergent-free solution has been investigated by static light-scattering and photon correlation spectroscopy. In detergent-free solution at 293.2 K, human transferrin receptor (hTfR) forms stable associates with a hydrodynamic radius of 16 nm. With increasing temperature the particles get more compact, above 340 K a phase transition takes, place and spontaneous aggregation of the receptor occurs. Under these conditions large clusters are formed that lead to fractal aggregates, coexisting with dendritic crystalline structures. The experimental findings are compatible with a model, which involves a reaction limited cluster-cluster aggregation mechanism in conjunction with a nucleation process. The molar enthalpy change associated with the phase transition was determined to be (1860 $\pm$ 150) kJ/mol^{-1} at a transition temperature of (341.3 $\pm$ 0.2) K.

INTRODUCTION

Aggregated and denatured states of proteins play an important role in the understanding of protein folding and stability, because in living organisms native and denatured states are in a dynamic equilibrium. Non-native states are also important for transporting proteins across membranes, proteolysis, and protein turnover (Dill and Shortle, 1991). Aggregation is also relevant for crystallization of proteins and for biotechnology, e.g., formation of inclusion bodies. However, information about denatured states and stability of membrane proteins is very limited (Stowell and Rees, 1995; Haltia and Freire, 1995).

Human transferrin receptor (hereafter abbreviated as hTfR) is a class II transmembrane glycoprotein (Turkewitz et al., 1988a), which is composed of two identical 90–95-kDa subunits (McClelland et al., 1984; Enns and Sussman, 1981). The subunits are linked by a disulfide bond, such that the major part of the molecule is exposed to the cell surface. Each subunit consists of a 61-residue cytoplasmic domain, a 28-residue membrane spanning region made up of hydrophobic amino acids, and a 760-residue extracellular domain with three N-glycosylation sites and one O-glycosylation site (Orberger et al., 1992). Each subunit possesses one transferrin binding site in the extracellular domain (Enns and Sussman, 1981; Schneider et al., 1982). In vertebrates, hTfR mediates the iron uptake by binding and internalization of the iron transport protein transferrin in its diferric state (ferri-transferrin). Upon endocytosis, the hTfR-transferrin complex becomes exposed to an acidic pH in the endosome. Under these conditions, the Fe^{3+} ions dissociate from the receptor-bound diferric transferrin and are transported into the cytosol. The receptor-transferrin complex recycles back to the cell surface, where the iron-free transferrin dissociates and is replaced by an iron-loaded one. Aggregation of hTfR possibly plays a role during endocytosis and recycling of the receptor. It might facilitate the formation of tubular structures involved in the recycling of hTfR to the cell surface. Those tubular structures have been identified in fibroblasts (Hopkins et al., 1994). Reticulocytes clear their plasma membrane from transferrin receptor upon maturation. In humans this is achieved by proteolytic cleavage of the extracellular domains leading to the soluble serum transferrin receptor (Shih et al., 1990). However, in sheep the excess transferrin receptor is removed from the cell surface by a different mechanism. Within certain multilamellar intracellular compartments the receptor aggregates in the form of spherical bodies and is released to the exterior by fusion of the vesicular membrane with the cell membrane (Pan et al., 1985).

Presently, only the biophysical and colloidal properties of a soluble 70-kD fragment of hTfR have been investigated in solution. The soluble 70-kD fragment, comprising 95% of the extracellular part of hTfR, can be produced by digestion of the receptor with trypsin (Turkewitz et al., 1988a). This fragment undergoes a reversible aggregation upon exposure to an acidic environment (pH 5.5) (Turkewitz et al., 1988b). This study was extended by Hadden et al. (1994), who investigated the thermal stability and temperature or pH change-induced conformational changes of the extracellular fragment of hTfR, using Fourier transform infrared spectroscopy (FTIR). On heating a solution of the extracellular fragment, they found differences in the FTIR spectra, which they attributed to a thermal denaturation of the molecule. A transition temperature of 70°C was determined for the onset of aggregation at pH 7.4, whereas structural changes occurred at 71°C under the same conditions. All these transitions seemed to be irreversible. Under acidic conditions the transition temperature decreased to 55°C.

Received for publication 8 September 1998 and in final form 19 May 1999.

Address reprint requests to Dr. Wolfram Saenger, Institut für Kristallographie, Freie Universität Berlin, Takustrasse 6, D-14195 Berlin, Germany. Tel.: +49-30-838-3412; Fax: +49-30-838-6702; E-mail: saenger@chemie.fu-berlin.de.

0006-3495/99/08/1117/09 $2.00

Both studies were undertaken with the extracellular fragment, which forms a noncovalent dimer in detergent-free solution. However, the complete receptor is also stable in detergent-free solution, where it forms radial symmetric assemblies composed of nine receptor dimers with an average hydrodynamic radius of 16 nm (Fuchs et al., 1995, 1998; Schüler, J., J. Frank, J. Behlke, W. Saenger, and Y. Georgalis, submitted for publication).

In order to investigate in greater detail the thermal stability and the temperature-dependent behavior of the complete receptor in detergent-free solution, we performed static light-scattering (SLS) and photon correlation spectroscopy (PCS) experiments in the temperature range between 293 and 340 K. To augment light-scattering experiments, circular dichroism (CD) and differential scanning calorimetry (DSC) measurements were carried out.

MATERIALS AND METHODS

hTfR purification

CNBr Sepharose and Sephacryl S-400 were purchased from Pharmacia (Frieburg, Germany). Desferral, ferri-transferrin, and Triton X-100 were obtained from Sigma (Deisenhofen, Germany); salts and buffer components were from Merck (Darmstadt, Germany). All these substances were used without further purification.

hTfR was purified from human placenta using a CNBr Sepharose/ferri-transferrin affinity column according to Turkewitz et al. (1988) with the following modifications: after removal of Fe^{3+} from the affinity column by 0.2 mM Desferral at pH 5.0, hTfR was eluted under nondenaturing conditions with 2 M KCl, 10 mM CHAPS in 50 mM HEPES, pH 7.5. The purity of the receptor was proved by SDS-PAGE (Fig. 1). The receptor was homogenous with respect to the SDS-PAGE, but with PCS larger aggregates of hTfR (hydrodynamic radius, R_h, ~100 nm) could be observed. To remove those aggregates the protein solution was further purified by gel filtration using a Sephacryl S-400 column. After this additional purification step no larger aggregates could be detected by PCS. All protein concentrations were determined using the Pierce BCA protein assay (Pierce, Rockford, IL).

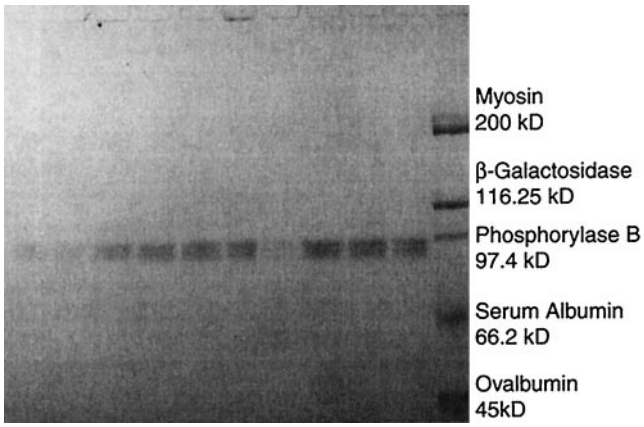

FIGURE 1 SDS-PAGE of purified hTfR. After elution from the affinity column, fractions were dialyzed against PBS, pH 7.5. Aliquots of each fraction were loaded on a 10% SDS-PAGE gel. Only bands for ~95-kD hTfR could be detected.

Sample preparation

For light-scattering experiments hTfR was diluted with PBS (phosphate buffered saline; 10 mM phosphate, 150 mM NaCl, pH 7.5) to a final concentration of 50 μg/ml. To remove dust, all samples were filtered through 200-nm pore size sterile filters (Minisart; Sartorius, Göttingen, Germany) before each measurement.

For CD spectroscopy the samples were dialyzed against a buffer containing 10 mM sodium cacodylate, pH 7.5, and 150 mM NaCl. The concentration of hTfR was adjusted to 50 μg/ml. Ferri-transferrin solutions were prepared the same way. Their final concentration was adjusted to give a 1:1 stoichiometry with respect to the concentration of binding sites.

For DSC experiments the hTfR solutions were concentrated to 4.5 mg/ml using Centriprep 30 units (Amicon; Beverly, MA) with a 30-kDa cutoff. The samples were extensively dialyzed against PBS. The same buffer served as reference during the DSC measurements.

Light scattering

Theory

The theory of light scattering has been reviewed in several monographs (Berne and Pecora, 1974; Schmitz, 1990; Brown 1993), so we give only a very basic introduction to the method. In a typical light-scattering experiment, a laser beam impinges on a solution and the scattered light is recorded by a photomultiplier. The spatial resolution of the experiment is defined by the scattering vector **q**, whose magnitude is given by the Bragg formula:

$$|\mathbf{q}| = \frac{4\pi n}{\lambda}\sin\left(\frac{\theta}{2}\right) \tag{1}$$

where λ denotes the wavelength of the scattered light, n the refractive index of the solution, and Θ the scattering angle.

In a PCS experiment the fluctuations of the scattered light due to the Brownian motion of the particles are analyzed in terms of an autocorrelation function (ACF), which is proportional to the distribution of relaxation times, τ, and scattering amplitudes of the examined components:

$$G^{(1)}(\tau) \propto \int_{R_{min}}^{R_{max}} N(R)M^2(R)P(\mathbf{q})S(\mathbf{q})\exp(-mR^{-1}\mathbf{q}^2\tau_{rel})\mathrm{d}R \tag{2}$$

where m is a proportionality constant, $N(R)$ and $M(R)$ denote number and mass of particles with radius R between the integration limits R_{min} and R_{max}, and $P(\mathbf{q})$ and $S(\mathbf{q})$ denote form and static structure factor of the particles. If the particles are small compared with the employed wavelength, the z-average translational diffusion coefficient, D, can be determined through Laplace inversion of the autocorrelation function. From D the hydrodynamic radii, R_h, of the particles are calculated according to the Stokes-Einstein equation:

$$R_h = \frac{k_B T}{6\pi\eta D} \tag{3}$$

where k_B denotes the Boltzmann constant, T the absolute temperature, and η the viscosity of the solvent.

In the case of large, asymmetric particles, rotational motions also contribute to the autocorrelation function. The magnitude of this effect can be roughly estimated according to Lindsay et al. (1988, 1989).

In an SLS experiment the time average intensity, $\langle I\rangle$, of the light scattered by the sample is recorded as a function of the scattering vector **q**. When examined on an appropriate spatial resolution,

$$1/R \ll |\mathbf{q}| \ll 1/r_0 \tag{4}$$

fractal aggregates, built up from monomers with radius r_0, usually show a power law dependence of the scattered intensity on the scattering vector:

$$\langle I\rangle(\mathbf{q}) \propto S(\mathbf{q})P_0(\mathbf{q}) \propto \mathbf{q}^p \quad (5)$$

were $P_0(\mathbf{q})$ denotes the form factor of the monomers.

The characteristic exponent, p, is associated with geometric properties of the particles and may take different values, depending on the spatial resolution (Martin, 1986; Schaefer et al., 1989). In the power law regime p can be expressed in terms of the mass fractal dimension, d_m, and the surface fractal dimension, d_s, according to:

$$p = 2d_m - d_s \quad (6)$$

A sample can exhibit mass or surface fractal properties depending on the spatial resolution of the experiment.

Experimental setup

PCS experiments were performed using an ALV SP-86 spectrogoniometer (Alvilangen, Germany). A Spectraphysics 165 Ar^+-Laser (488 nm) served as light source. Signals were recorded with a Thorn EMI D 191 A photomultiplier and, after amplification and discrimination, further processed by an ALV-5000 digital correlator board. Intensity ACFs were automatically recorded on 302 channels, quasi-logarithmically spaced in time. Theoretically, these channels cover a dynamic range between 12.5 ns and 3200 s. In practice, the lower limit is some 100 ns, due to dead-time distortions of the photomultiplier, and the upper limit is ~0.5 s, when short accumulation times are employed (i.e., 30–60 s per spectrum). The experiments were conducted at a scattering angle of 20°, corresponding to a scattering vector of 5.96×10^{-3} nm^{-1}. ACF spectra were Laplace-inverted by CONTIN (Provencher, 1982a, b) running on a Silicon Graphics workstation, using a 45-point logarithmic quadrature grid, non-negativity constraints, and the appropriate form factors for hard spheres. Due to the large amount of recorded spectra only the "best" solutions found by CONTIN (i.e., those having a probability of rejection close to 0.5) were considered. Rotational motions were decoupled as described by Georgalis et al. (1995).

SLS experiments were conducted on the same spectrogoniometer. Intensities were recorded between 20° and 150°, corresponding to scattering vectors between 5.96×10^{-3} nm^{-1} and 3.32×10^{-2} nm^{-1}. Intensities were integrated for 15 s at each angle and five scans were averaged for each experiment. The change of the scattering volume as a function of scattering angle, θ, was compensated by multiplying the initially set accumulation times of 15 s by a factor $\sin(\theta)$. Temperature was kept constant using a Lauda RC6 thermostat. For experiments involving linear temperature gradients this thermostat was used in combination with a Lauda P-351 programmable gradient driver. Viscosity and refractive index corrections for water at various temperatures were made through interpolation of data taken from standard tables (CRC Handbook of Chemistry and Physics, 1984–1985). The small differences between the buffer and pure water were neglected.

CD spectroscopy

CD spectra between 195 and 250 nm were recorded using a Jasco J-600 spectropolarimeter. All experiments were conducted using a cell with an optical pathlength of 2 mm. A scan speed of 5 nm/min and a step size of 0.2 nm were used throughout. Temperature was kept constant by a Lauda RC6 thermostat. For obtaining the final spectra, five individual runs were averaged.

DSC

DSC experiments of hTfR were performed using a MicroCal MC-2 differential scanning calorimeter (MicroCal, Northampton, MA) applying a scan rate of 30 K/h. The heat capacity C_p was measured as a function of temperature between 313.2 and 358.2 K. C_p was converted to the molar heat capacity C_p^m, accounting for the cell volume (1.2249 ml) and the sample concentration. The phase transition temperature T_m for hTfR was obtained from DSC curves after baseline subtraction at the highest value of the molar heat capacity C_p^m. The area under the DSC curve corresponds to the molar enthalpy change ΔH_{cal} for the phase transition.

Light microscopy

Images of the hTfR clusters were recorded with an Axiovert 100 inverted microscope (Zeiss, Germany) employing a long-distance objective (Achrostigmat 32X, Zeiss). The overall magnification of the images was determined by calibration with standard grids. Observations were made directly in the light-scattering cells at room temperature ~18 h after completion of the light-scattering experiments. Images were acquired by using a black-and-white CCD camera.

RESULTS

Temperature-induced aggregation of hTfR in detergent-free solution was examined by PCS using linear temperature gradients. In Fig. 2 *A*, values of the apparent hydrodynamic radius, R_h, obtained by PCS are plotted as a function of the temperature. Temperature was raised from 293.2 to 340.2 K with a rate of 0.21 K/min. Then it was kept constant at 340.2 K. At 293.2 K hTfR associates with an average value for R_h of 16 nm could be detected. With increasing temperature the hydrodynamic radius of the clusters decreased. After reaching the final temperature we observed an aggregation process leading to aggregates with a radius above 1 μm. Further evidence for a temperature-induced aggregation at 340.2 K is presented in Fig. 2, *B* and *C*, where autocorrelation functions and corresponding radius distributions are presented. Here the experiment was performed at 340 K, e.g., no temperature gradient was applied. The autocorrelation functions (Fig. 2 *B*) obtained at different times after the start of the measurement are shifted to longer relaxation times. This indicates an increase of the radius of the observed particles, as can be seen in Fig. 2 *C*.

In Fig. 3 *A* the time course of the average hydrodynamic radius at 340.2 K is shown. After ~50 min, clusters reach a radius of 50 nm. Beyond this point, the aggregates grow further according to a power law. This is obvious from the linear dependence between radius and time in a double-logarithmic plot. A slope of 1.91 ± 0.02 is obtained from this curve. The onset of the aggregation, displayed in greater detail in Fig. 3 *B*, shows that the particles grow exponentially during the first 50 min. The slope of the regression line is $(5.13 \pm 0.08)\ 10^{-4}$ s^{-1} and the intercept (13 ± 1) nm.

In Fig. 4 *A* a double-logarithmic plot displays the time-averaged total intensity of the scattered light, $\langle I\rangle$, against the hydrodynamic radius measured during the temperature-induced aggregation at 340.2 K. The experiment was performed at a 20° scattering angle. From the slope of the linear part of this plot the mass fractal dimension, d_m, can be estimated (Pusey and Rarity, 1987) as:

$$\ln(\langle I\rangle) \propto d_m \ln(R_h) \quad (7)$$

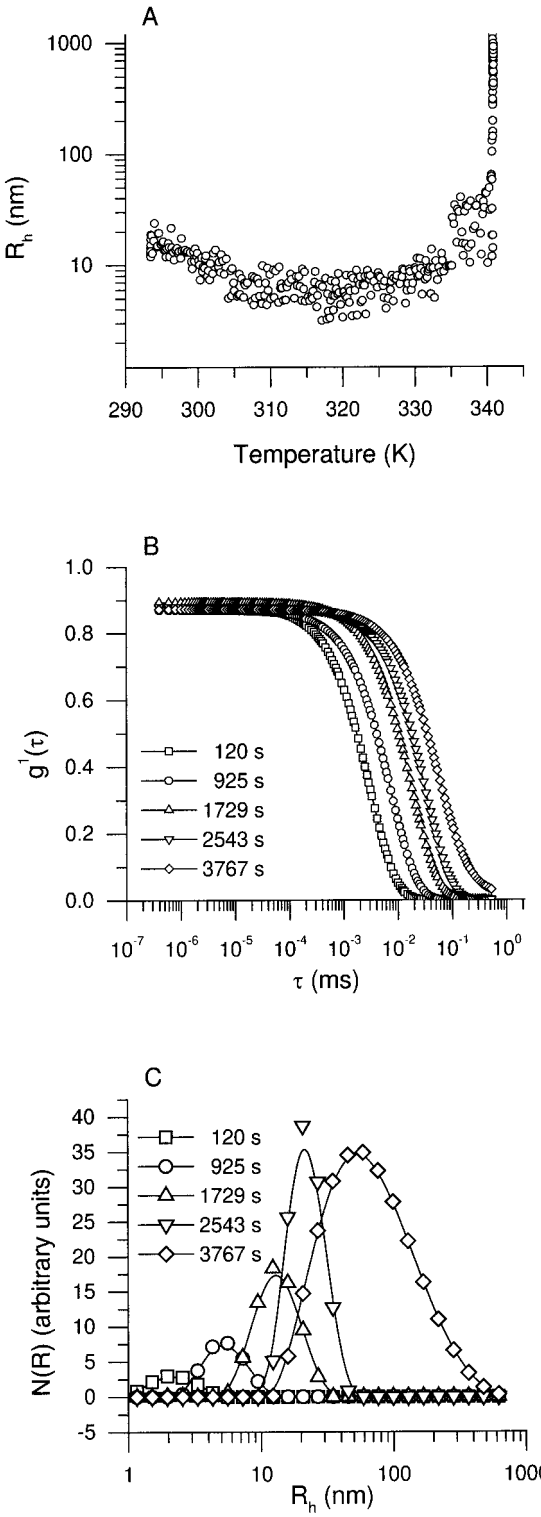

FIGURE 2 (*A*) Temperature-dependence of the apparent hydrodynamic radii of hTfR in PBS, pH 7.5. Temperature was raised from 293.2 to 340.2 K with a rate of 0.21 K/min and then kept constant. After reaching a minimum at ~320 K, the hydrodynamic radii increased at 340.2 K. (*B*) Autocorrelation functions measured at several times after heating the hTfR solution to 340.2 K. All curves were measured at a scattering angle of 20°. The relaxation times shift to higher values with time, indicating an aggregation process. (*C*) Particle radius distributions obtained through Laplace inversion of the autocorrelation functions with CONTIN. The hydrodynamic radii and the polydispersity increase with time.

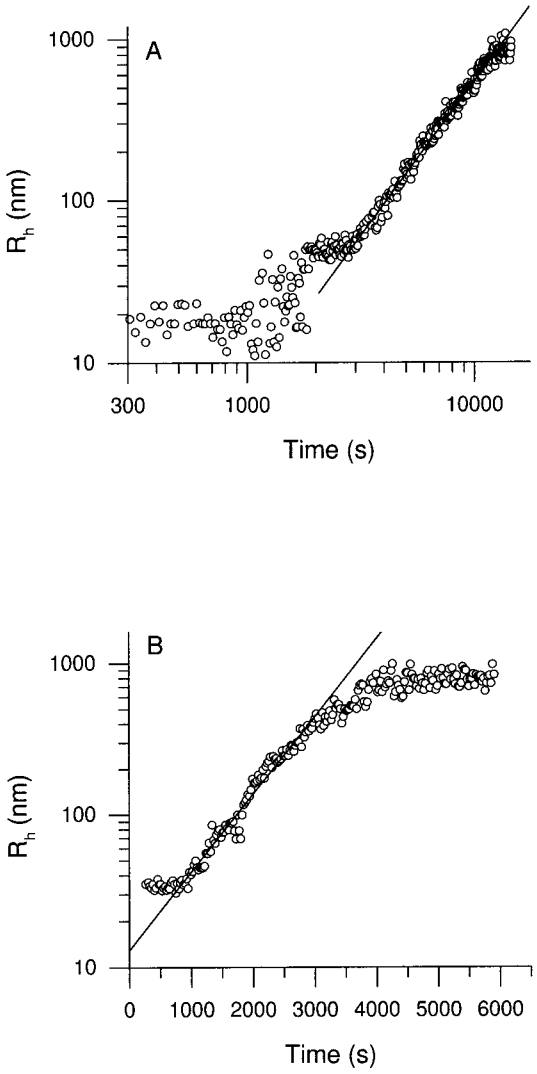

FIGURE 3 (*A*) Double-logarithmic plot of the hydrodynamic radii as function of time. After a lag period, there is a power law dependence between radius and time. The slope of the regression line is (1.91 ± 0.02). (*B*) Semilogarithmic plot of the hydrodynamic radius versus the aggregation time. Here the onset of the aggregation is displayed in greater detail. The linear part of the plot indicates an exponential growth, compatible with an RLCA mechanism. The fit delivers a value of (13 ± 1) nm for the hydrodynamic radius of the seed particles.

For particle sizes between 40 and 150 nm the slope was determined to be 2.18 ± 0.03. When the particles get larger the assumptions leading to Eq. 7 are no longer valid, and the curve deviates from linearity.

In Fig. 4 *B* $\langle I \rangle / P_0(\mathbf{q})$ is double-logarithmically plotted against the scattering vector. The form factor of the monomers, $P_0(\mathbf{q})$, was calculated according to Kerker (1969), assuming that the monomers can be approximated as homogeneous spheres:

$$P_0(\mathbf{q}) = \frac{9}{(qr_0)^6}(\sin qr_0 - qr_0 \cos qr_0)^2 \qquad (8)$$

The experiment was performed at a later stage of the aggregation, where the radii of the clusters are larger than the

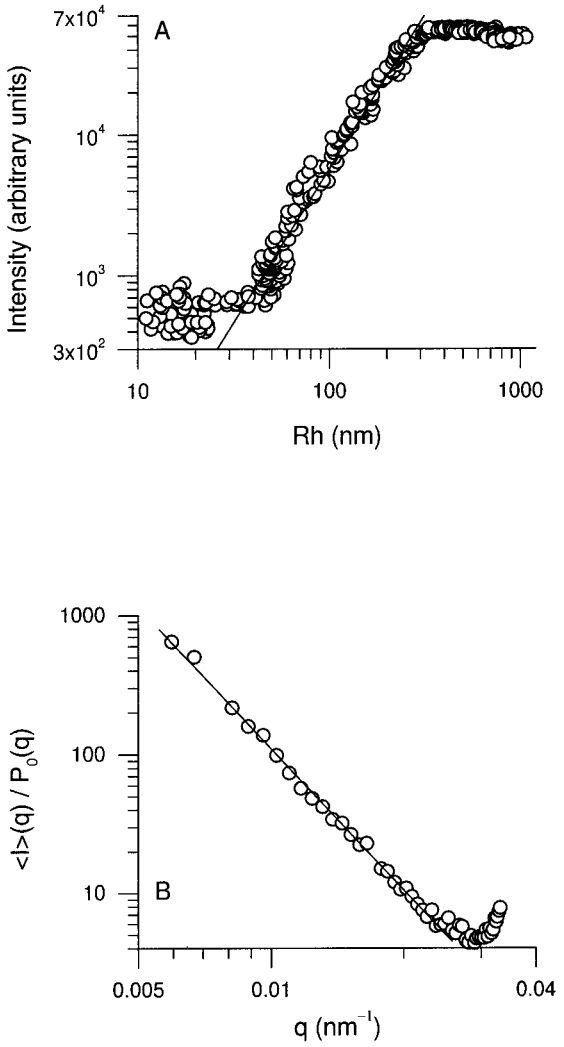

FIGURE 4 (*A*) Double-logarithmic plot of the hydrodynamic radii versus the intensity of the scattered light during the early phase of the aggregation at 340.2 K. The PCS experiment was performed at a scattering angle of 20°. The slope of the regression line is (2.18 ± 0.03), indicative of a RLCA mechanism. (*B*) Scattering vector-dependence of the scattered intensity. The data were measured at a later stage of the aggregation. The slope of the regression line is −(3.38 ± 0.04).

wavelength of the light. Fig. 4 *B* clearly indicates a power law dependence of $\langle I \rangle / P_0(\mathbf{q})$ on the scattering vector. From the slope of the regression line a characteristic exponent of −(3.38 ± 0.04) can be derived.

Upon completion of the light-scattering experiments the samples were cooled down to room temperature and examined after 18 h under a light microscope. To our surprise we observed not only fractal aggregates but also crystalline structures, which showed optical birefringence. In Fig. 5 *A* typical fractal clusters are displayed. The radius of the clusters is ~5 μm; they seem to consist of small compact building units (*inset*). In Fig. 5 *B* small crystalline particles are displayed. They have a somewhat dendritic shape and exhibit optical birefringence. Sadly, the microcrystals did not grow any further and attempts to use them as seed particles in crystallization experiments failed.

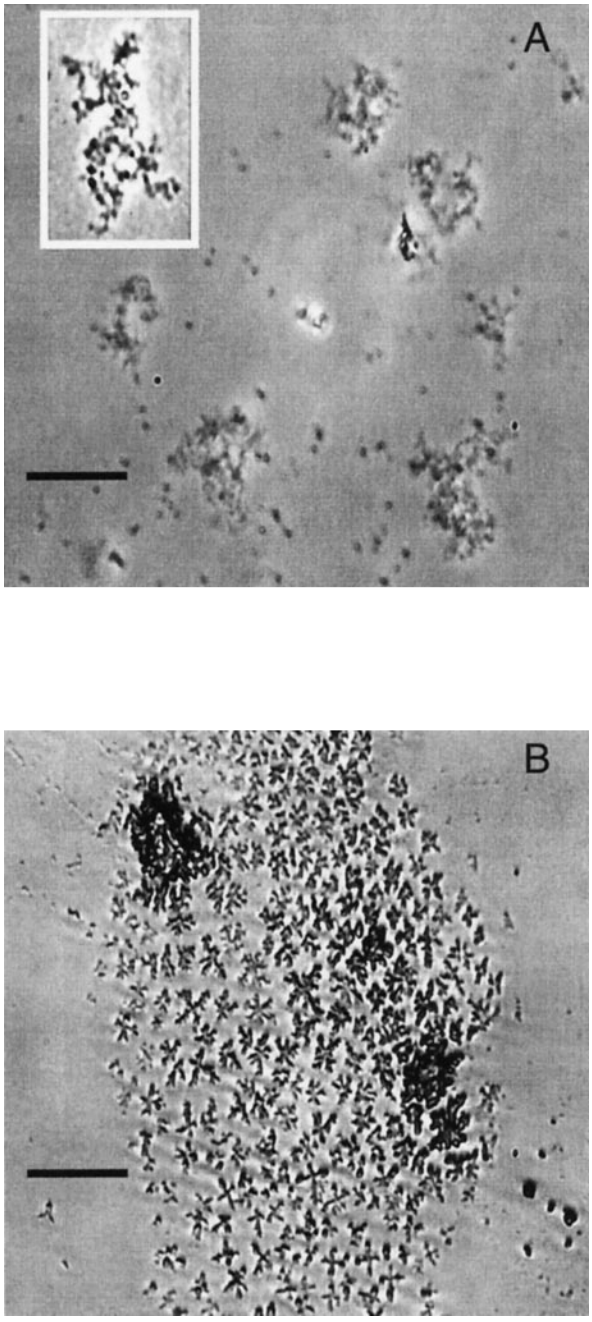

FIGURE 5 Light microscopic images of hTfR clusters in PBS, pH 7.5. After completion of the aggregation experiment, the solution was cooled down to room temperature and images were recorded 18 h later. We observed fractal aggregates (*A*); in the inset a single cluster is displayed at higher magnification. The fractal clusters coexist with dendritic aggregates, which showed optical birefringence (*B*).

As the growth of the hTfR clusters led to crystalline structures, we have followed the time course of the characteristic exponents to get more information on the growth process. In Fig. 6 *A* double-logarithmic plots of $\langle I \rangle / P_0(\mathbf{q})$ against **q** for different times after starting the aggregation are displayed. From the first few records it is evident that one can visualize two different slopes. This can be attributed to at least two different growth processes, which occur on

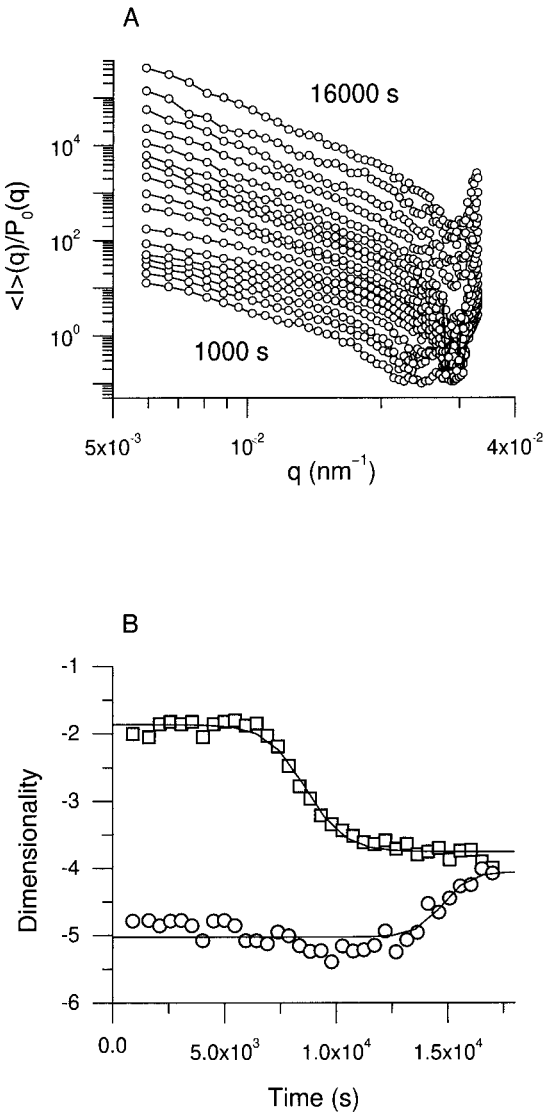

FIGURE 6 (*A*) Time course of an aggregation experiment at 340.2 K between 1000 and 16,000 s after initiation, followed by static light scattering. The individual spectra are shifted by ascending powers of 2. Two different slopes could be extracted from linear regression to each curve segment, involving some 15 points each. (*B*) Characteristic exponents determined from the slopes of the spectra depicted in (*A*). Both curves show a sigmoidal behavior. At later stages both slopes collapse at a value of −4.

different length scales. The time course of the scaling exponent of each segment can be determined by a linear regression to each set of data, Fig. 6 *B*. The determined exponents of the first process start at values close to −2.05 and asymptotically approach the value of −4.0. Similarly, the values of the second exponent start from −5.0 and asymptotically relax to the same value of −4.0.

To estimate the amount of conformational change associated with higher temperatures, CD spectra of hTfR at various temperatures were recorded (Fig. 7 *A*). At 298.2 K the spectrum displays two minima at ~208 and 222 nm. Such spectra are usually indicative for proteins with a high number of α-helical regions (Manavalan and Johnson, 1983). When raising the temperature to 328.2 K, 348.2 K, and finally to 363.2 K, both maxima decreased. This effect was more pronounced for the peak at 208 nm. The temperature-dependent changes in CD spectra indicate some structural changes, although it is questionable whether a complete denaturation of the protein takes place. A spectrum recorded at 363.2 K after denaturation of the protein by 1% SDS is displayed for comparison in Fig. 7 *A*. Here the peak at 208 nm is vastly diminished, and the peak at 222 nm has almost disappeared. Fig. 7 *B* shows CD spectra of the complex between hTfR and its ligand transferrin at 298.2 K and 348.2 K. As expected, the complex shows a slightly different CD spectrum from the free receptor. Interestingly, the complex seems to be more stable than hTfR alone, which is indicated by the similarity of the spectra taken at 298.2 and 348.2 K.

DSC experiments show a single phase transition for hTfR with a transition temperature, T_m, of (341.3 ± 0.2) K (Fig. 7 *C*). The molar enthalpy change ΔH associated with the phase change was determined to be (1860 ± 150) kJ/mol^{-1}.

DISCUSSION

Aggregation phenomena can be formulated in terms of fractal dimensions, which characterize the geometric properties of the aggregates and provide information about the kinetics of the aggregation process. During the last years this concept has been applied to the aggregation of proteins by several authors (Feder et al., 1984; Horne, 1987; Rarity et al., 1989; Georgalis et al., 1993).

The kinetics of colloidal aggregation depend on a balance of attractive and repulsive forces among the interacting species. If only attractive forces are present, each encounter between two particles leads to aggregation. The kinetics of this process only depend on the diffusion rate of the particles, therefore this regime is called diffusion-limited colloidal aggregation (DLCA) (Lin et al., 1990). The apparent hydrodynamic radius depends on time according to a simple power law:

$$R_h(t) = R_0(1 + Ct)^{z/d_m} \quad (9)$$

where R_0 is the hydrodynamic radius of a seed particle, C is a constant characteristic for the observed system, and t is the aggregation time. The sticking probability, z, is per definition one in the case of DLCA. The fractal dimension, d_m, can be obtained from the slope of a double-logarithmic plot of the apparent hydrodynamic radius as a function of time. For aggregation in the DLCA regime a universal fractal dimension of 1.8 is observed (Weitz and Oliveria, 1984; Weitz et al., 1985; Weitz and Lin, 1986).

If repulsive forces are present, then several encounters are necessary for aggregate formation. The kinetics of the aggregation process depend on the rate of successful encounters between the particles. This mechanism therefore is called reaction-limited colloidal aggregation (RLCA). The

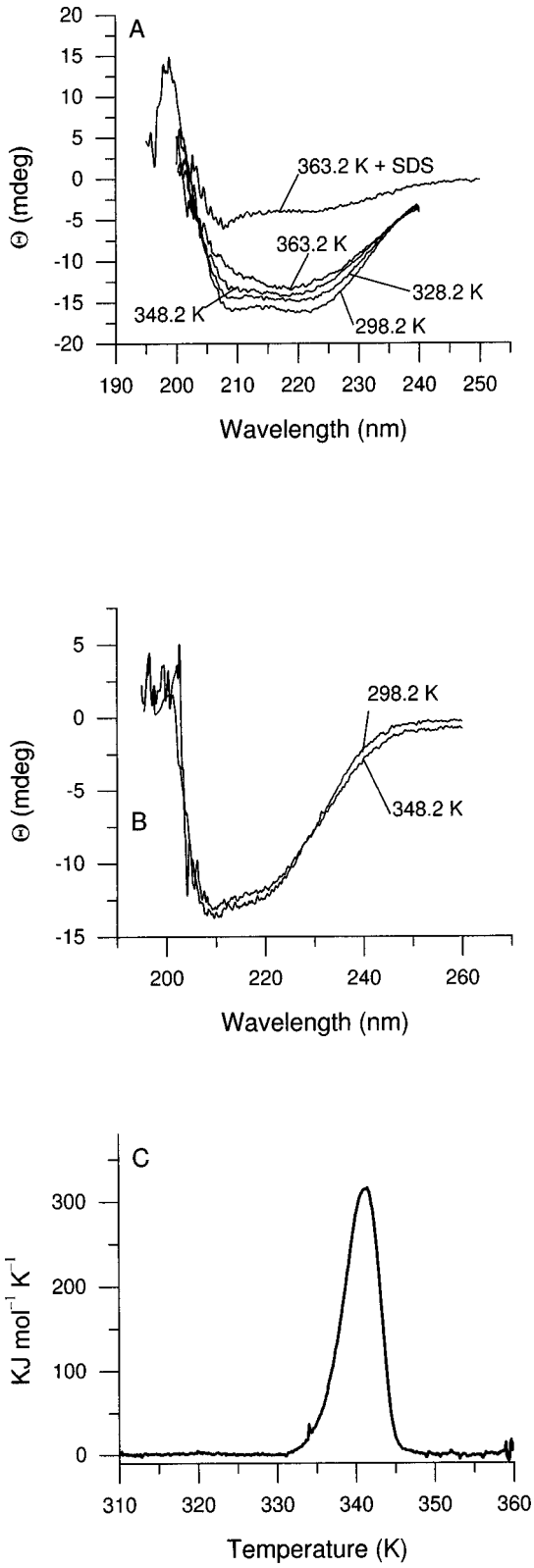

FIGURE 7 (*A*) CD spectra of hTfR in 10 mM sodium cacodylate buffer, pH 7.5 at various temperatures. The spectra show some decrease of the minima at 208 and 222 nm, indicative of some conformational changes at higher temperatures. For comparison also a spectrum of hTfR is displayed after denaturation with 1% SDS at 363.2 K. (*B*) CD spectra of the complex between hTfR and its ligand ferri-transferrin at 298.2 and 348.2 K. The differences between the two spectra are smaller than the differences observed in the case of unliganded hTfR, Fig. 7 *A*. (*C*) Differential scanning calorimetry (DSC) experiment for the temperature-induced phase transition of hTfR. The measurement delivered only one peak with a transition temperature of (341.3 ± 0.2) K. The molar enthalpy change associated with the phase transition was determined to be (1860 ± 150) kJ/mol^{-1}.

hydrodynamic radius of the particles increases exponentially with time:

$$R_h(t) = R_0 \exp(C\alpha t) \quad (10)$$

where α is the sticking probability on impact.

It is obvious that the fractal dimension cannot be determined directly from Eq. 10, so other evaluation schemes must be employed. A typical value of the fractal dimension for clusters formed in the RLCA regime is 2.1 (Lin et al. 1989, 1990).

In detergent-free solution hTfR forms associates with an apparent hydrodynamic radius of 16 nm at 293.2 K. With increasing temperature the particles get more compact and the apparent hydrodynamic radius reaches a minimum at ~320 K (Fig. 2 *A*). At 340.2 K aggregation is induced. The time course of the aggregation process can be easily followed by PCS, as shown in Fig. 2, *B* and *C*. The autocorrelation functions at various stages of the reaction are clearly separated and the size distribution of the particles can be derived from them. However, it should be noted that the polydispersity of the aggregates also increases with time (Fig. 2 *C*). To determine the mechanism of the aggregation, further experiments were performed at 340.2 K.

For a DLCA mechanism, the fractal dimension can be determined from the slope of a double-logarithmic plot of the hydrodynamic radius against time. For our system this plot delivers a growth exponent of 1.9 ± 0.02 for the later stages of the aggregation, which is clearly not compatible with a DLCA mechanism (to obtain a fractal dimension of 1.8 the exponent should be 0.56). The data rather suggest a power law dependence between the apparent hydrodynamic radius of the aggregates and the reaction time for the later stages of the reaction. Thus, from the simple plot displayed in Fig. 3 *A* no clues concerning the growth mechanism at this stage can be drawn. The situation is further complicated by the increasing polydispersity of the sample (Fig. 2 *C*), which has a great impact on the accuracy of the radius determination (Martin and Ackerson, 1985; Martin and Leyvraz, 1986).

During the onset period, the hydrodynamic radius grows exponentially with time. This behavior is indicative for an RLCA mechanism (Fig. 3 *B*). A nonlinear fit according Eq. 10 delivers a seed particle size of (13 ± 1) nm, which is in a good agreement with the size of the hTfR associates determined at 293.2 K, and a value of (5.13 ± 0.08) 10^{-4} s^{-1} for the product $C\alpha$.

To directly determine the fractal dimension of the clusters at the early stage of the aggregation, the intensity of the scattered light was plotted as a function of the hydrodynamic radius of the particles (Fig. 4 *A*). From a fit to the

linearized data, the fractal dimension can be determined to be (2.18 ± 0.03), which gives further evidence for an aggregation according to an RLCA mechanism. The geometric properties of particles for which $\mathbf{q}R > 1$ can be determined from the dependence of the scattered light on the scattering vector, which delivers a characteristic exponent depending on the size and structure of the particles and the spatial resolution of the experiment. For our system, we obtain an exponent of $-(3.38 \pm 0.04)$ (Fig. 4 *B*). Such a non-integer value has also been reported for experiments with silica aggregates (Schaefer et al., 1984) and lignite coal (Bale and Schmidt, 1984), and is associated with scattering from porous particles. As stated in Eq. 6, the exponent depends on the fractal dimension of the aggregates visible at the investigated length scale. When the particles exhibit a homogenous mass distribution their mass fractal dimension is just 3, and Eq. 6 can be written as:

$$p = 6 - d_s \tag{11}$$

where d_s is the surface fractal dimension and describes the roughness of the aggregates. For smooth particles the surface fractal dimension equals 2 and an exponent of -4 is expected, whereas the highest value the surface fractal dimension can reach is 3. In our case we obtain a surface fractal dimension of 2.62.

After 18 h at room temperature we examined our samples under a light microscope. Besides the expected large fractal clusters (Fig. 5 *A*), small dendritic crystalline structures were also observed (Fig. 5 *B*). To explain the formation of crystalline structures, some sort of a nucleation process must be assumed, which involves the formation of homogeneously dense particles with a smooth surface (Schaefer et al., 1989). To get a more detailed picture of the process, we performed time-dependent SLS experiments. The data were plotted in the same manner as in Fig. 4 *B*. Especially the first curves, obtained after 1000 s, show that there are two slopes present, whose values could be extracted (Fig. 6 *A*). The time course of the two slopes is displayed in Fig. 6 *B*. The upper curve starts at ~ -2 and approaches -4. The lower curve starts at -5 and also approaches -4. This may be interpreted in terms of a coexistence of at least two species. In the first, small smooth particles are surrounded by interfacial layers (in the presence of interfacial layers the surface fractal dimension can be <2), which evolve to larger particles with an apparently smooth surface. In the second, RLCA type aggregates undergo restructuring and get more and more compact and finally yield smooth and uniformly dense structures. This surely oversimplified picture is supported by studies on the crystallization of zeoliths (Dokter et al., 1995). In this system the slopes of the scattering curves started at ~ -1.5 and later approached a value of -4, which was interpreted in terms of two restructuring steps leading to the formation of crystalline structures.

To assess the influence of increasing temperature on the conformational stability of hTfR, we measured CD spectra of the protein at different temperatures. With rising temperature the number of α-helical regions in the protein seems to decrease. In comparison with the spectra taken after SDS treatment, the changes seem to be quite moderate, at least in the temperature range employed for the light-scattering experiments. However, this cannot rule out denaturation, since it has been shown for several membrane proteins that denaturation is not necessarily associated with global conformational changes (Haltia and Freire, 1995). Membrane-spanning parts of the proteins especially resist thermal unfolding, whereas the extracellular parts are more likely to undergo conformational changes. The DSC experiment delivers only one transition temperature, which is slightly higher than the temperature where aggregation and nucleation are initiated. Consequently, the question whether the protein investigated by light scattering is already denatured is not easy to answer. The highest temperature used for light-scattering experiments was 1 K below the transition temperature determined by DSC. Feder et al. (1984) have shown for the thermally induced aggregation of immunoglobulin (IgG), that even for temperatures sufficient for aggregation, there is still ~60% of the protein in a native state. Thus we conclude that there is a fairly high amount of undenatured material present at 340.2 K. This is also supported by the formation of crystalline structures, which is usually not observed with denatured material.

Aggregation cannot only be induced thermally, but also by lowering the pH of the solution. At pH 5 aggregation takes place even at room temperature (Schüler et al., submitted for publication; see above). Under this condition, hTfR forms large aggregates with apparent hydrodynamic radii between 80 and 2000 nm. Due to the high polydispersity of the solution, it was not possible to identify distinct components. SLS experiments lead to a characteristic exponent of $-(3.48 \pm 0.07)$, which is similar to the exponent observed during the later stages of the thermally induced aggregation at pH 7.5 (Fig. 4 *B*). This implies that under both conditions similar structures are formed and that the aggregation may be described by the same model.

Colloidal aggregation depends basically on a balance between packing attractive London and repulsive Coulomb forces among the interacting species. On the basis of this simplified picture, the aggregation of hTfR can be explained by the following scheme: in detergent-free solution at pH 7.5, hTfR forms small aggregates. The isoelectric point of the receptor is 5.2 (Schneider et al., 1982) suggesting that the molecules possess a negative surface charge. Aggregation is prevented by repulsive forces, which are higher than the thermal energy of the particles. With increasing temperature more and more collisions between particles lead to aggregation. Upon pH shift from 7.5 to 5.0, negatively charged residues become more and more protonated, leading to a lowering of repulsive forces and finally to aggregation.

The membrane-spanning regions of membrane proteins are usually resistant against thermal unfolding, whereas the extracellular parts behave more like globular proteins (Stowell and Rees, 1995; Haltia and Freire, 1995). Therefore, local unfolding of regions in the extracellular domain

of hTfR may lead to the exposure of hydrophobic sites to the surface, which facilitates aggregation. Probably both mechanisms contribute to the observed thermally induced aggregation dynamics and the crystallization phase transition of hTfR.

The authors thank Prof. Dr. J. F. Holzwarth (Fritz Haber Institut, Berlin) for providing us with the facilities for DSC measurements. The support by the staff of the maternity ward, Frauen- und Polyklinik, Charité Campus Virchow Klinikum, Berlin is deeply acknowledged.

REFERENCES

Bale, H. D., and P. W. Schmidt. 1984. Small-angle x-ray-scattering investigation of submicroscopic porosity with fractal properties. *Phys. Rev. Lett.* 53:596–599.

Berne, B. J., and R. Pecora. 1974. Dynamic Light Scattering. Wiley, New York.

Brown, W. 1993. Dynamic Light Scattering, the Method and Some Applications. Oxford Science Publications, London.

CRC Handbook of Chemistry and Physics, 65th ed. 1984/85. The Chemical Rubber Company, Cleveland.

Dill, K. A., and D. Shortle. 1991. Denatured states of proteins. *Annu. Rev. Biochem.* 60:795–825.

Dokter, W. H., H. F. van Garderen, T. P. M. Beelen, R. A. van Santen, and W. Brass. 1995. Homogene und heterogene Kristallkeimbildung bei Zeolithen. *Angew. Chem.* 107:122–125; *Angew. Chem. Int. Ed. Engl.* 34:73–75.

Enns, C. A., and H. H. Sussman. 1981. Physical characterization of the transferrin receptor in human placenta *J. Biol. Chem.* 256:9820–9823.

Feder, J., T. Jøssang, and E. Rosenqvist. 1984. Scaling behaviour and cluster fractal dimension determined by light scattering from aggregation proteins. *Phys. Rev. Lett.* 53:1403–1406.

Fuchs, H., R. Gessner, R. Tauber, and R. Gosh. 1995. Functional reconstitution of the human placental transferrin receptor into phospholipid bilayers leads to long tubular structures proceeding from the vesicle surface. *Biochemistry*. 34:6196–6207.

Fuchs, H., U. Lücken, R. Tauber, a. Engel, and R. Gessner. 1998. Structural model of phospholipid-reconstituted human transferrin receptor derived by electron microscopy. *Structure.* 6:1235–1243.

Georgalis, Y., J. Schüler, J. Frank, M. D. Soumpasis, and W. Saenger. 1995. Protein crystallization screening through light-scattering techniques. *Adv. Colloid Interface Sci.* 58:57–86.

Georgalis, Y., A. Zouni, W. Eberstein, and W. Saenger. 1993. Formation dynamics of protein precrystallization fractal clusters. *J. Cryst. Growth*. 126:245–260.

Hadden, J. M., M. Bloemendal, P. I. Haris, I. H. M. van Stokkum, D. Chapman, and S. K. S. Srai. 1994. Structure and thermal stability of the extracellular fragment of human transferrin receptor at extracellular and endosomal pH. *FEBS Lett.* 350:235–239.

Haltia, T., and E. Freire. 1995. Forces and factors that contribute to the structural stability of membrane proteins. *Biochim. Biophys. Acta*. 1228: 1–27.

Hopkins, C. R., A. Gibson, M. Shipman, D. K. Strickland, and I. S. Trowbridge. 1994. In migrating fibroblasts, recycling receptors are concentrated in narrow tubules in the pericentriolar area, and then routed to the plasma membrane of the leading lamella. *J. Cell Biol.* 125: 1265–1274.

Horne, D. S. 1987. Determination of the fractal dimension using turbidimetric techniques. *Faraday Discuss. Chem. Soc.* 83:259–270.

Kerker, M. 1969. The Scattering of Light. Academic Press, New York.

Lin, M. Y., H. M. Lindsay, D. A. Weitz, R. C. Ball, R. Klein, and P. Meakin. 1989. Universality of fractal aggregates as probed by light scattering. *Proc. R. Soc. Lond. A.* 423:71–87.

Lin, M. Y., H. M. Lindsay, D. A. Weitz, R. Klein, R. C. Ball, and P. Meakin. 1990. Universal diffusion-limited colloid aggregation. *J. Phys.: Condens. Matter*. 2:3093–3113.

Lindsay, H. M., R. Klein, D. A. Weitz, M. Y. Lin, and P. Meakin. 1988. Effect of rotational diffusion on quasielastic light scattering from fractal colloid aggregates. *Phys. Rev. A.* 38:2614–2626.

Lindsay, H. M., R. Klein, D. A. Weitz, M. Y. Lin, and P. Meakin. 1989. Structure and anisotropy of colloid aggregates. *Phys. Rev. A.* 39: 3112–3119.

Manavalan, P., and W. C. Johnson, Jr. 1983. Sensitivity of circular dichroism to protein tertiary structure class. *Nature.* 305:831–832.

Martin, J. E. 1986. Scattering exponents for polydisperse surface and mass fractals. *J. Appl. Crystallogr.* 19:25–27.

Martin, J. E., and B. J. Ackerson. 1985. Static and dynamic scattering from fractals. *Phys. Rev. A.* 31:1180–1182.

Martin, J. E., and F. Leyvraz. 1986. Quasielastic-scattering linewidths and relaxation times for surface and mass fractals. *Phys. Rev. A.* 34: 2346–2350.

McClelland, A., L. C. Kuhn, and F. H. Ruddle. 1984. The human transferrin receptor gene: genomic organization and the complete primary structure of the receptor deduced from a cDNA sequence. *Cell.* 39: 267–274.

Orberger, G., R. Geyer, S. Stirm, and R. Tauber. 1992. Structure of the N-linked oligosaccharides of the human transferrin receptor. *Eur. J. Biochem.* 205:257–267.

Pan, B. T., K. Teng, W. Choan, M. Adam, and R. M. Johnstone. 1985. Electron microscopic evidence for externalization of the transferrin receptor in vesicular form in sheep reticulocytes. *J. Cell Biol.* 101: 942–948.

Provencher, S. W. 1982a. A constrained regularization method for inverting data represented by linear algebraic or integral equations. *Comp. Phys. Comm.* 27:213–227.

Provencher, S. W. 1982b. CONTIN: A general purpose constrained regularization program for inverting noisy linear algebraic and integral equations. *Comp. Phys. Comm.* 27:229–242.

Pusey, P. N., and J. G. Rarity. 1987. Measurement of the hydrodynamic fractal dimension of aggregating polystyrene spheres. *Mol. Phys.* 62: 411–418.

Rarity, J. G., R. N. Seabrook, and R. J. G. Carr. 1989. Light-scattering studies of aggregation. *Proc. R. Soc. Lond. A.* 423:89–102.

Schaefer, D. W., B. C. Bunker, and J. P. Wilcoxon. 1989. Fractals and phase separation. *Proc. R. Soc. Lond. A.* 423:35–53.

Schaefer, D. W., J. E. Martin, P. Wiltzius, and D. S. Cannell. 1984. Fractal geometry of colloidal aggregates. *Phys. Rev. Lett.* 52:2371–2374.

Schmitz, S. K. 1990. An Introduction to Dynamic Light Scattering by Macromolecules. Academic Press, New York.

Schneider, C., R. Sutherland, R. Newman, and M. Greaves. 1982. Structural features of the cell surface receptor for transferrin that is recognized by the monoclonal antibody OKT9. *J. Biol. Chem.* 257:19077–19801.

Shih, Y. J., R. D. Baynes, B. G. Hudson, C. H. Flowers, B. S. Skikne, and J. D. Cook. 1990. Serum transferrin receptor is a truncated form of tissue receptor. *J. Biol. Chem.* 265:19077–19081.

Stowell, M. H. B., and D. C. Rees. 1995. Structure and stability of membrane proteins. *Adv. Protein Chem.* 46:279–311.

Turkewitz, A. P., J. F. Armatruda, D. Borhani, S. C. Harrison, and A. L. Schwartz. 1988a. A high yield purification of the human transferrin receptor and properties of its major extracellular fragment. *J. Biol. Chem.* 263:8318–8325.

Turkewitz, A. P., A. L. Schwartz, and S. C. Harrison. 1988b. A pH-dependent reversible conformational transition of the human transferrin receptor leads to self-association. *J. Biol. Chem.* 263:16309–16315.

Weitz, D. A., and M. Y. Lin. 1986. Dynamic scaling of cluster-mass distribution in kinetic colloid aggregation. *Phys. Rev. Lett.* 57: 2037–2040.

Weitz, D. A., M. Y. Lin, and C. J. Sandroff. 1985. Colloidal aggregation revisited: new insights based on fractal structure and surface enhanced Raman scattering. *Surface Sci.* 158:147–164.

Weitz, D. A., and M. Oliveria. 1984. Fractal structures formed by kinetic aggregation of aqueous gold colloids. *Phys. Rev. Lett.* 52:1433–1436.